European Journal of Medicinal Chemistry 87 (2014) 429–439

Contents lists available at ScienceDirect

European Journal of Medicinal Chemistry

journal homepage: http://www.elsevier.com/locate/ejmech

Original article

Discovery of indanone derivatives as multi-target-directed ligands against Alzheimer's disease

Ling Huang, Hui Miao, Yang Sun, Fanchao Meng, Xingshu Li*

School of Pharmaceutical Sciences, Sun Yat-sen University, Guangzhou 510006, China

ARTICLE INFO

Article history:
Received 4 March 2014
Received in revised form
20 August 2014
Accepted 24 September 2014
Available online 26 September 2014

Keywords:
Indanone derivatives
Alzheimer's disease
Acetylcholinesterase inhibitors
Amyloid beta
Antioxidant

ABSTRACT

A series of indanone derivatives were designed, synthesized, and tested using a variety of assays to assess their potential as anti-Alzheimer's disease (AD) agents. The investigations assessed the activities of the agents for the inhibition of cholinesterases (AChE and BuChE), the inhibition of amyloid beta (Aβ) self-assembly, and the catalysis of the disassembly of preformed Aβ oligomers and measured their antioxidant activities. Our results demonstrate that most of the synthesized compounds demonstrated good inhibitory activity against AChE with IC_{50} values in the nanomolar range. In particular, compounds **9** (IC_{50} = 14.8 nM) and **14** (IC_{50} = 18.6 nM) exhibited markedly higher inhibitory activities than tacrine and similar activities to donepezil. In addition, **9** and **14** significantly inhibited Aβ aggregation (inhibition rates of 85.5% and 83.8%, respectively), catalysed the disaggregation of Aβ fibrils generated by self-induced Aβ aggregation, and exhibited antioxidant activity. Furthermore, these two compounds can cross the blood–brain barrier (BBB) in vitro. These properties highlight the potential of these new compounds to be developed as multi-functional drugs for the treatment of Alzheimer's disease.

1. Introduction

Alzheimer's disease (AD), a chronic neurodegenerative disorder characterized by memory loss and other cognitive impairments, is the most prevalent cause of dementia in the elderly and affects millions of people around the world [1]. Over the last two decades, a great amount of research studies focused on deciphering the underlying mechanisms of AD. Although the aetiology of AD remains elusive, multiple factors, such as β-amyloid (Aβ), τ-protein, oxidative stress, dyshomeostasis of biometals, and low levels of acetylcholine, likely play important roles in the development of AD [2].

Based on the correlation of the reduction of cholinergic activity in the central nervous system (CNS) of AD patients with their degree of cognitive function disorder, the 'cholinergic hypothesis' was proposed [3]. As a result, cholinesterase (ChE) became one of the major targets in the current therapy of AD [4]. In fact, four out of the five approved drugs for AD are acetylcholinesterase inhibitors (AChEIs). These include tacrine, donepezil, rivastigmine, and galantamine, all of which have beneficial effects on the cognitive, functional, and behavioural symptoms of AD. However, the current treatments for AD are only able to treat symptoms of the disease and do little to stop or reverse the progression. The amyloid hypothesis, which is another hypothesis for the aetiology of AD, states that the accumulation of Aβ in the brain is the primary factor that drives AD pathogenesis [5]. Moreover, candidate drugs that are intended to reduce Aβ production, prevent Aβ aggregation, and promote Aβ clearance are currently in clinical trials [6]. In addition, Aβ deposits inflict oxidative injury in the surrounding neurons and elicit an acute inflammatory response, which contributes to the neurodegeneration observed in AD [7]. Indeed, an increasing body of evidence confirming the presence of reactive oxygen species (ROS)- and reactive nitrogen species (RNS)-mediated injury in AD brains suggests a pivotal role of oxidative stress in the pathogenesis of AD [8]. Moreover, human observational epidemiology studies are, in general, consistent with the hypothesis that there is an inverse relationship between antioxidant levels and intake, cognitive function, and ultimately the risk of developing AD [9]. Thus, the development of antioxidants is thought to be a beneficial approach for the treatment of AD.

Recent evidence indicates that the "one molecule, multiple targets" paradigm is effective for the treatment of complex diseases due to the drug's ability to interact with multiple targets responsible for the pathogenesis of the disease. Given the complex nature of AD and the fact that a single drug acting on a specific target (AChE) may have undesirable clinical effects, the "one molecule,

* Corresponding author.
E-mail address: lixsh@mail.sysu.edu.cn (X. Li).

http://dx.doi.org/10.1016/j.ejmech.2014.09.081
0223-5234/

multiple targets" paradigm strategy has also been applied in anti-AD drug design and was recently proven to be a successful strategy for the treatment of this multifaceted disease by a large body of evidence [10]. The results of these previous studies suggest that this multifunctional approach may advance the discovery of novel therapeutics to prevent or slow down the progression of AD more efficiently and effectively.

In a previous work, we developed a series of indanone derivatives [11] (representative compound A; Fig. 1) and benzylideneindanone derivatives [12] (representative compound B; Fig. 1) that were proven to be efficient AChE inhibitors and Aβ aggregation inhibitors, respectively. Following the "one molecule, multiple targets" design strategy, herein, we designed another series of indanone derivatives by rationally combining the AChE inhibitory pharmacophore of compound A and the Aβ aggregation inhibitory pharmacophore of compound B into a single molecule (Fig. 1) and thereby expected to produce multifunctional anti-AD agents that simultaneously target cholinesterase activity and amyloid aggregation.

2. Results and discussion

2.1. Chemistry

The synthetic approach used for the generation of our new indanone derivatives is illustrated in Scheme 1. Commercially available ferulic acid **1** was hydrogenated in the presence of Pd/C, cyclized at 120 °C, and then catalysed by methanesulfonic acid to obtain the indanone **3** with a 70% yield. The alkylation of **3** with different dibromoalkane compounds in acetonitrile provided **4a**–**4d** with 60–75% yields, and these compounds were then treated with piperidine to yield **5a**, **5b**, **5d**. Finally, the target compounds **6**–**15** were obtained by the direct condensation of **5a**, **5b**, **5d** and the appropriate substituted aldehydes in a methanolic NaOH solution, which resulted in the formation of the desired compound as a precipitate that was separated by filtration and further purified by chromatography on silica gel. Substituted aldehydes (wherever not commercially available) were prepared by the aminomethylation of 4-fluorobenzaldehyde in the presence of tetrabutylammonium bromide (TBAB) according to a previously reported procedure [13]. Commercially available cyclohexylamine was reacted with **4a**–**4d** to give the corresponding intermediates **16a**–**16c**, which were then condensed with 4-(dimethylamino) benzaldehyde to afford **17a**–**17c** at a yield of 75–82%. Derivative 18 was prepared in good yield (86%) by reacting **5a** with 4-methoxybenzaldehyde in the presence of NaOH at room temperature. The E configuration at the double bond was by NOESY spectra of compound **6** (See Supplementary data), which is consistent with the configuration of reported indanone aldol condensation product [14]. These target compounds were characterized by their melting point and ^{1}H NMR, ^{13}C NMR, and HRMS spectra. The chemical purities (>95%) of compounds **6**–**15**, **17a**–**17c**, and **18**, were confirmed by HPLC.

2.2. In vitro inhibition of AChE and BuChE

The AChE (*Electrophorus electricus*, *ee*AChE) inhibitory effects of the newly synthesized compounds were determined through the spectroscopic method described by Ellman et al. [15]. using tacrine and donepezil as the standards. The results are summarized in Table 1. As expected, most of the synthesized compounds demonstrated good inhibitory activity against AChE with IC_{50} values in the nanomolar range. In particular, compounds **6** (IC_{50} = 16.5 nM), **9** (IC_{50} = 14.8 nM), **12** (IC_{50} = 16.8 nM), **13** (IC_{50} = 25.5 nM), **14** (IC_{50} = 18.6 nM), **15** (IC_{50} = 14.6 nM), and **18** (IC_{50} = 14.8 nM), which contain a piperidine group linked to an indanone moiety through two carbons, exhibited markedly higher activity than tacrine and similar activity to donepezil. Surprisingly, the replacement of the piperidine group with a cyclohexylamine group markedly decreased the inhibitory activity, i.e., **6** (IC_{50} = 16.5 nM) vs. **17a** (IC_{50} = 102 nM), **7** (IC_{50} = 330.3 nM) vs. **17b** (IC_{50} = 1540.3 nM), and **8** (IC_{50} = 1032.1 nM) vs. **17c** (IC_{50} = 9181.3 nM). A structure–activity relationship analysis showed that the inhibitory potency against AChE is closely related with the length of the linker and with the group linked at the 6th-position of the indanone moiety. The variation in the length of the linker between piperidine and the indanone moieties significantly influenced the AChE inhibitory activities. The compounds with a two-carbon linker (**6** and **9**) appeared to exhibit more potent activity than those with three-carbon (**7** and **10**) and five-carbon linkers (**8** and **11**). For example, compound **9** (IC_{50} = 14.8 nM) displayed much more potent AChE inhibitory activity than compounds **10** (IC_{50} = 371.0 nM) and **11** (IC_{50} = 5729.1 nM). However, the substitution of the benzyl moiety appeared to have no relevant role in

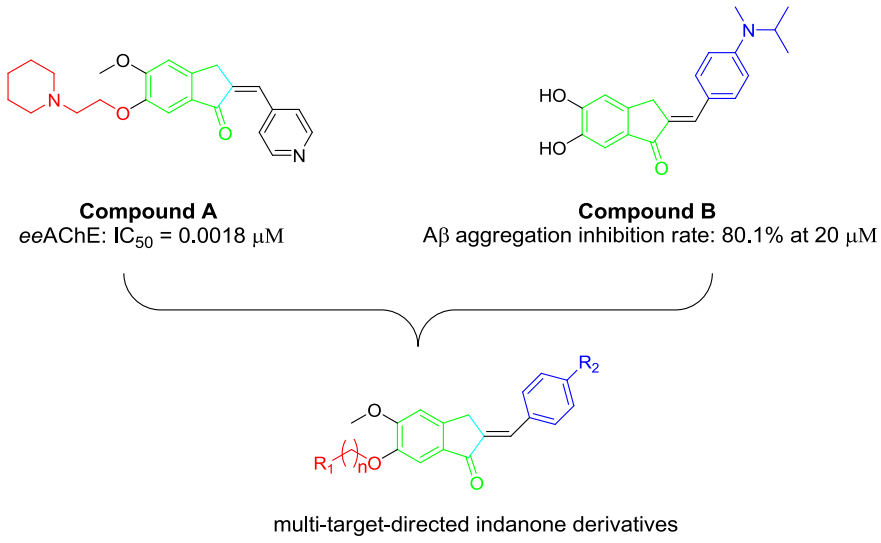

Fig. 1. Design strategy for multi-target-directed indanone derivatives.

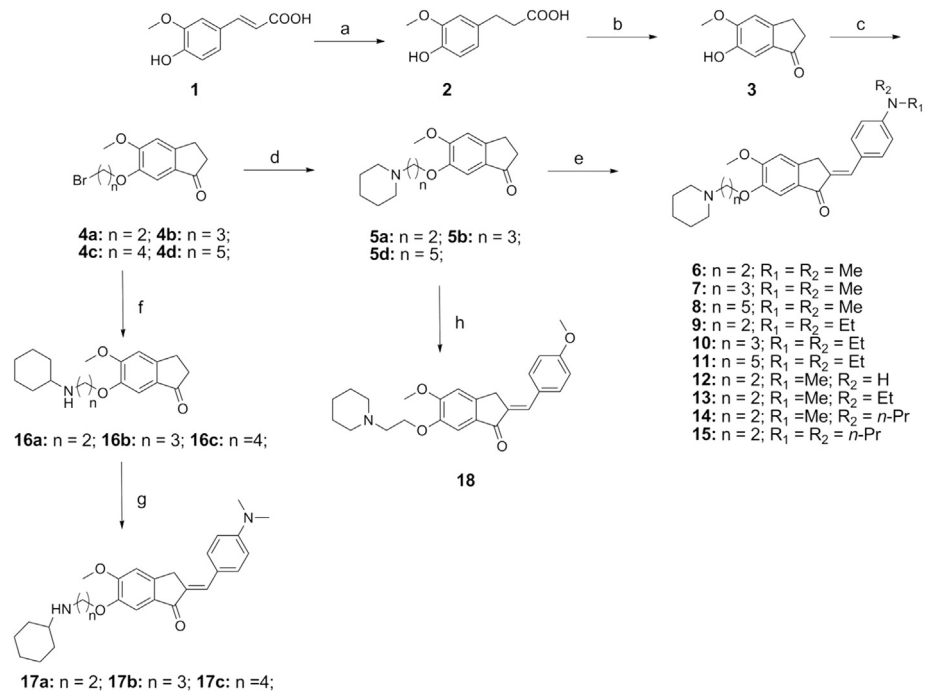

Scheme 1. Synthesis of Target Compounds **6**–**15**, **17a**–**17c**, and **18**. Reagents and conditions: (a) Pd/C, H_2, MeOH, 40 °C; (b) Methanesulfonic acid, 120 °C; (c) $Br(CH_2)_nBr$, K_2CO_3, acetonitrile, 80 °C; (d) piperidine, acetonitrile, 80 °C; (e) appropriate benzaldehyde, NaOH, MeOH, rt; (f) cyclohexylamine, acetonitrile, 80 °C; (g) 4-(dimethylamino)benzaldehyde, NaOH, MeOH, rt; (h) 4-methoxybenzaldehyde, NaOH, MeOH, rt.

Table 1
In vitro inhibition of AChE and BuChE and oxygen radical absorbance capacity (ORAC, Trolox equivalents) of **6**–**15**, **17a**–**17c**, **18**, donepezil, and tacrine.

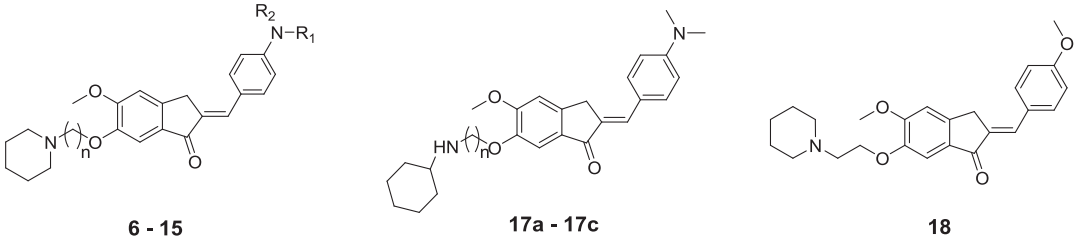

Comp.	*n*	R_1	R_2	IC_{50} (nM) eeAChE[a]	IC_{50} (nM) eqBuChE[b]	Selectivity for AChE[c]	IC_{50} (nM) hAChE[d]	ORAC
6	2	Me	Me	16.5 ± 0.6	1493.8 ± 134	90.5	285.1 ± 7.8	3.55 ± 0.31
7	3	Me	Me	330.3 ± 2.6	1457.1 ± 108	4.4	Nd	2.40 ± 0.08
8	5	Me	Me	1032.1 ± 41.3	2441.2 ± 235	2.4	Nd	2.88 ± 0.16
9	2	Et	Et	14.8 ± 1.0	1384.9 ± 80	93.6	536.4 ± 15.9	3.70 ± 0.32
10	3	Et	Et	371.0 ± 17.2	2817.4 ± 234	7.6	nd[e]	1.86 ± 0.08
11	5	Et	Et	5729.1 ± 107.8	2843.8 ± 38	0.50	Nd	1.67 ± 0.16
12	2	Me	H	16.8 ± 0.1	1640.2 ± 92	97.6	301.1 ± 3.3	3.30 ± 0.19
13	2	Me	Et	25.5 ± 1.2	127 1.1 ± 133	49.8	426.0 ± 17.9	3.88 ± 0.33
14	2	Me	n-Pr	18.6 ± 0.1	1417.1 ± 65	76.2	390.2 ± 17.4	3.40 ± 0.10
15	2	n-Pr	n-Pr	14.6 ± 0.1	1769.9 ± 149	121.2	954.2 ± 54.0	2.66 ± 0.16
17a	2	Me	Me	102.0 ± 1.2	363.5 ± 32	3.6	nd	3.03 ± 0.10
17b	3	Me	Me	1540.3 ± 235.4	1326.9 ± 83	0.86	nd	2.74 ± 0.26
17c	4	Me	Me	9181.3 ± 22.0	1129.8 ± 14	0.12	nd	3.54 ± 0.13
18	–	–	–	14.8 ± 0.8	3213.6 ± 323	217.0	nd	0.15 ± 0.01
Donepezil	–	–	–	38.2 ± 3.1	3365.4 ± 61	88.1	11.7 ± 1.1	nd
Tacrine	–	–	–	109 ± 10.31	15.2 ± 2	0.14	285.0 ± 29.4	nd

[a] 50% inhibitory concentration (means ± SD of three experiments) of AChE from electric eel.
[b] 50% inhibitory concentration (means ± SD of three experiments) of BuChE from equine serum.
[c] Selectivity for AChE = IC_{50} (eqBuChE)/IC_{50} (eeAChE).
[d] 50% inhibitory concentration (means ± SD of three experiments) of AChE from human erythrocytes.
[e] Not determined.

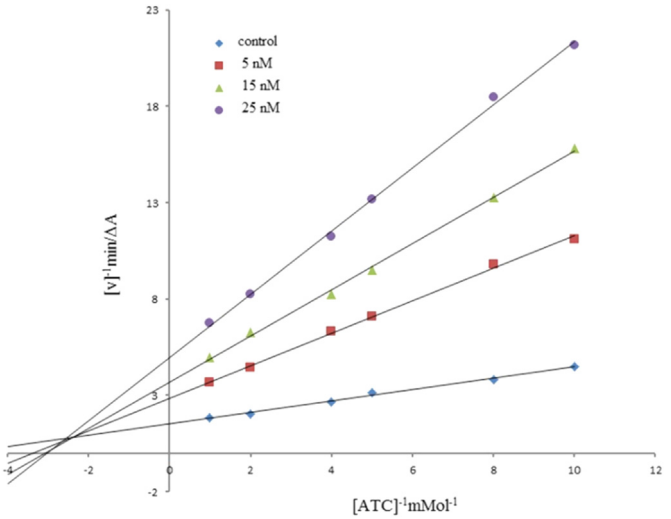

Fig. 2. Steady state inhibition by compound **9** of AChE hydrolysis of ACh; the plots show mixed-type inhibition for compound **9** on AChE.

the enzymatic activity. For instance, compounds **6** (IC_{50} = 16.5 nM), **9** (IC_{50} = 14.8 nM), **15** (IC_{50} = 14.6 nM), and **18** (IC_{50} = 14.8 nM), which contain a dimethylamino group, diethylamino group, di-*n*-propylamino group, and methoxy group at the *para*-position of the benzyl moiety, respectively, exhibited similar inhibitory activities against AChE. The in vitro BuChE (equine serum) inhibition was also determined using the same method. Most of the newly synthesized compounds demonstrated slightly higher inhibitory potency against BuChE than donepezil.

2.3. In vitro inhibition of hAChE

Because of human AChE (*h*AChE) is more appropriate, we also evaluated the inhibition activity of compounds **6**, **9**, **12**, **13**, **14**, and **15** against hAChE using the same method that was used to evaluate the *ee*AChE inhibitory activity. As shown in Table 1, all of the tested compounds showed weaker inhibition activities against *h*AChE than that against AChE from electric eel. Of the tested compounds, **6** showed the best inhibition activity against hAChE with an IC_{50} of 285.1 nM, which is similar to the activity of tacrine (IC_{50} = 285.0 nM). Similar to the *ee*AChE inhibition activity, the substitution in the benzyl moiety did not obviously affect the activity. Although compounds **9** (IC_{50} = 534.6 nM), **12** (IC_{50} = 301.1 nM), **13** (IC_{50} = 426.0 nM), and **14** (IC_{50} = 390.2 nM) exhibited similar inhibitory activities, we chose **9** and **14** for further study based on their inhibitory activity against $A\beta_{1-42}$ aggregation.

2.4. Kinetic study of AChE

In order to investigate the mechanism of indanone derivatives against AChE, kinetic study was performed using compound **9** and the steady-state inhibition data of it for AChE is shown in Fig. 2. Lineweaver–Burk reciprocal plots revealed that there was an increasing slope and an increasing intercept at higher inhibitor concentrations, indicating the mixed inhibition. Based on the kinetic analysis, we concluded that indanone derivatives exhibited as dual binding sites AChE inhibitors, which targeting simultaneously catalytic and peripheral sites of AChE.

2.5. Molecular modelling studies

Molecular docking simulations have become important tools in recent years for gaining insight into the interaction mode and the structure–activity relationships of ligands with drones. To study the possible interaction mode between the indanone derivatives and AchE, molecular docking simulations were performed using the CDOCKER program in the Discovery studio 2.1 software. Compounds **9** and **14** docked to the TcAChE active site cavity based on the structure of the *T. californica* enzyme complex (TcAChE; PDB entry 2CMF). The docking and subsequent scoring were performed using the default parameters of the CDOCKER program. The binding gorge of TcAChE composed of the catalytic active site (CAS) and a peripheral anionic site (PAS) were taken as the binding site for docking and the most likely conformations of the ligand were selected based on the calculated docking score for the bonding strength. As shown in Fig. 3a, Compounds **9** and **14** demonstrated similar interaction models with AChE, both of them could favourably interact with the CAS and the PAS along the active-site gorge of the enzyme with its three major functional groups. The benzyl rings of **9** and **14** reached the top of the cavity and interacted with PAS residue Trp279 (3.53 Å and 4.126 Å, respectively) through π–π stacking. Near the bottom of the gorge, the protonated piperidine moiety of compounds **9** and **14** might interact with Phe330 and Trp84 via hydrophobic interactions to form a cation–π interaction. Meanwhile, the indanone moiety snaked along the gorge, interacting with Val71, Ser122, Phe331, Tyr121 and Tyr334 by hydrophobic and π–π interactions. Compounds **10**, **11** and **17a** were also

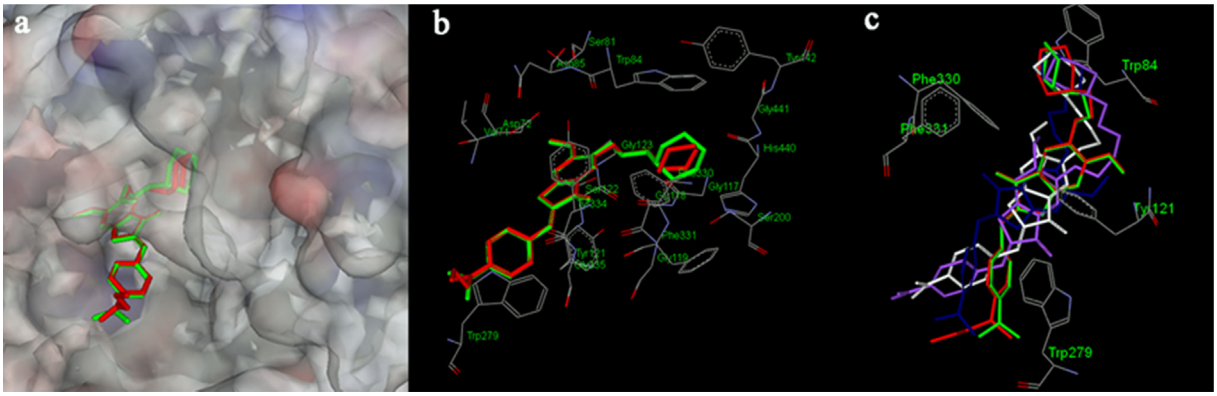

Fig. 3. Docking models of the compound–enzyme complex. (a): stereoviews looking down the gorge of TcAChE binding with **9** (green) and **14** (red). a: (b):compounds **9** (green) and **14** (red) docked into the catalytic gorge of TcAChE, highlighting the protein residues belonging to ACS and PAS that establish the main interactions. (c): superposition of modelled structure of compound **9** (green), **10** (blue), **11** (purple), **14** (red) and **17a**(white). (For interpretation of the references to colour in this figure legend, the reader is referred to the web version of this article.)

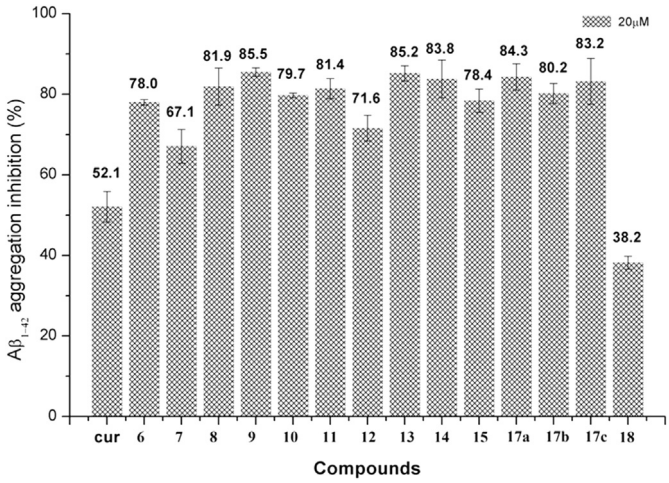

Fig. 4. Effects of the indanone derivatives on $A\beta_{1-42}$ peptide aggregation inhibition. The derivatives were used at a concentration of 20 μM.

docked into active sit of AChE using the same modelling method. The superposition of modelled structures (Fig. 3c) showed that all of them cloud interact with CAS and PAS of AChE through piperidine moiety (cyclohexylamine moiety of **17a**) and benzyl moiety, respectively. However, to make piperidine moiety could interact with CAS, the compounds **10**, **11** and **17a** adopted a twisted conformation, which was supposed to increase the interaction energy of ligand and enzyme. These results could explain the decrease of inhibition with the cyclohexyl moiety or the length of the linker.

2.6. In vitro antioxidant activity

The antioxidant activities of the target compounds were determined through the oxygen radical absorbance capacity assay using fluorescein (ORAC-FL) according to the method originally described by Ou et al. [16] and modified by Dávalos et al. [17], which was thought to be most appropriate methods for evaluating antioxidant as drugs. The vitamin E analogue Trolox was used as the standard, and the antioxidant activity is expressed as Trolox equivalents (μmol of Trolox/μmol of tested compound). As shown in Table 1, all of the derivatives with the exception of compound **18** demonstrated excellent antioxidant activity with ORAC-FL values of 1.67–3.88 Trolox equivalents. Compound **13**, which possesses an ethyl(methyl) amino at the para-position of the benzyl moiety, was the strongest antioxidant (ORAC-FL value of 3.88). It is surprising that the replacement of the amino group at the para-position of the benzyl moiety with the methoxy group resulted in an almost complete loss of the antioxidant activity to only 0.15 Trolox equivalents. These results suggest that the inclusion of an amino group in the benzyl moiety contributes to the radical scavenging ability of the hybrids.

2.7. Inhibition of self-mediated $A\beta_{1-42}$ aggregation by ThT

$A\beta_{1-40}$ and $A\beta_{1-42}$ are the main forms of Aβ peptides found in amyloid plaques and are released from an amyloid precursor protein through sequential cleavages by β- and γ-secretases. Although $A\beta_{1-40}$ is the predominant product of this proteolytic pathway, $A\beta_{1-42}$ is markedly more fibrillogenic [18]. Therefore, we chose to use $A\beta_{1-42}$ to study the inhibition activity of the hybrid compounds. The ability of the novel hybrids to inhibit $A\beta_{1-42}$ aggregation was assessed by the thioflavin T fluorescence assay using curcumin as the standard. The presence of aggregated $A\beta_{1-42}$ fibrils can be monitored by the fluorescence emission of ThT, which is a histochemical dye that binds to the predominant secondary structure of Aβ fibrils. As shown in Fig. 4, most of the target compounds exhibited markedly higher inhibitory activity than curcumin. Surprising, the $A\beta_{1-42}$ aggregation inhibition rate of compound **18**, which has a methoxy group in the benzyl moiety, was significantly less than that of the amino-substituted indanone derivatives, which indicates that the substitution groups are crucial for the inhibitory activity. Of the compounds, **9**, **13**, **14**, and **17a** showed high inhibitory activity with 85.5%, 85.2%, 83.8%, and 84.3% inhibition rates, respectively. Thus, we further investigated the multi-target profiles of compounds **9** (diethylamino group on the benzyl moiety, IC_{50} = 14.8 nM against *ee*AChE, IC_{50} = 526.4 nM against *h*AChE, ORAC = 3.70) and **14** (3,5-dihydroxy group on A ring, IC_{50} = 18.6 nM against *ee*AChE, IC_{50} = 390.2 nM against *h*AChE, ORAC = 3.40) based on their AChE inhibition and antioxidant activities.

2.8. Inhibition of $A\beta_{1-42}$ fibril formation monitored by transmission electron microscopy (TEM)

To complement the results of the ThT binding assay, the inhibitory activities of compounds **9** and **14** on $A\beta_{1-42}$ fibril formation were monitored by transmission electron microscopy (TEM). As shown in Fig. 3, after 24 h of incubation at 37 °C, $A\beta_{1-42}$ alone aggregated into well-defined Aβ fibrils (Fig. 5a). In contrast, few Aβ fibrils were observed in the presence of compounds **9** and **14** (Fig. 5b, c) under identical conditions. These results indicate that compounds **9** and **14** can inhibit and slow down the aggregation of $A\beta_{1-42}$ into fibrils, which is consistent with the results of the ThT assay.

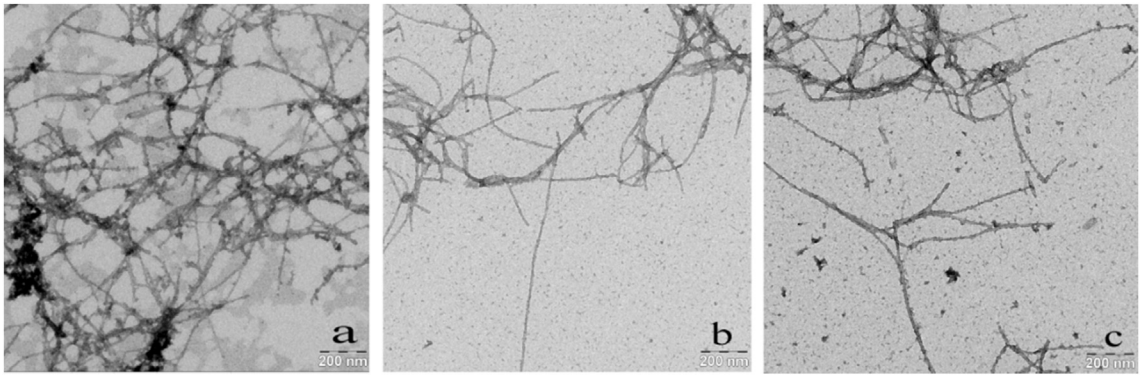

Fig. 5. TEM image analysis of $A\beta_{1-42}$ aggregation in the presence of **9** and **14**. (a) $A\beta_{1-42}$ alone (25 μM) was incubated at 37 °C for 24 h; (b) $A\beta_{1-42}$ (25 μM) and **9** (20 μM) were incubated at 37 °C for 24 h; (c) $A\beta_{1-42}$ (25 μM) and **14** (20 μM) were incubated at 37 °C for 24 h.

2.9. Disaggregation of $A\beta_{1-42}$ aggregation fibrils by **9** and **14**

In the normal human brain, Aβ is produced as a nontoxic soluble peptide. However, Aβ aggregates and accumulates in the AD brain as inert diffuse plaques or compact plaques associated with neurodegenerative changes. It has been proven that the neurotoxicity of the amyloid peptide is associated with amyloid fibrils [19]. To further study the multifunctional properties of the target compounds, the ability of **9** and **14** to disaggregate self-induced Aβ aggregation fibrils was investigated through the ThT binding assay and the TEM method. The Aβ fibrils were first generated by incubating fresh Aβ for 24 h at 37 °C. The test compounds were individually added to the samples, and the mixtures were incubated for 24 h at 37 °C (Fig. 6A). As shown in Fig. 4B, the ThT binding assay demonstrated that both **9** and **14** can disaggregate Aβ fibrils with disaggregation rates of 65.0% and 73.8, respectively. The TEM images shown in Fig. 6C demonstrate that the fresh Aβ was well-aggregated into Aβ fibrils (Fig. 6C, a) after incubation for 24 h at 37 °C. The number of fibrils was significantly decreased after incubation of the fibrils with **9** and **14** for 24 h, which supports the results of the ThT binding assay.

2.10. In vitro blood–brain barrier permeation assay

It is well known that the permeability of the blood–brain barrier (BBB) is one of the major hurdles for the successful development of CNS drugs [20]. To evaluate the in vitro BBB permeability of **9** and **14**, the parallel artificial membrane permeation assay of the blood–brain barrier (PAMPA-BBB) described by Di et al. was performed. This protocol allows us to predict the passive BBB permeation with high success, high throughput, and high reproducibility [21]. First, we compared the permeability of 13 commercial drugs with reported values to validate the assay (data are shown in Table 2). A plot of the experimental data versus the reported values produced a good linear correlation: Pe(exp) = 1.4574Pe (lit) − 1.0773 ($R^2 = 0.9427$; Fig. 7). Using this equation and considering the

Table 2
Permeability ($P_e \times 10^{-6}$ cm s^{-1}) of 13 commercial drugs used for the experimental validation of the PAMPA-BBB assay.

Commercial drugs	Bibl[a]	PBS:EtOH (70:30)[b]
Testosterone	17	22.3 ± 1.4
Verapamil	16	21.2 ± 1.9
Desipramine	12	16.4 ± 1.2
Progesterone	9.3	17.7 ± 1.2
Promazine	8.8	14.3 ± 0.5
Chlorpromazine	6.5	6.0 ± 0.3
Clonidine	5.3	5.1 ± 0.3
Piroxicam	2.5	0.24 ± 0.01
Hydrocortisone	1.9	0.65 ± 0.01
Lomefloxacin	1.1	0.37 ± 0.02
Atenolol	0.8	0.78 ± 0.02
Ofloxacin	0.8	0.37 ± 0.02
Theophylline	0.1	0.26 ± 0.01

[a] Obtained from reference 21.
[b] The data are the means ± SD of three independent experiments.

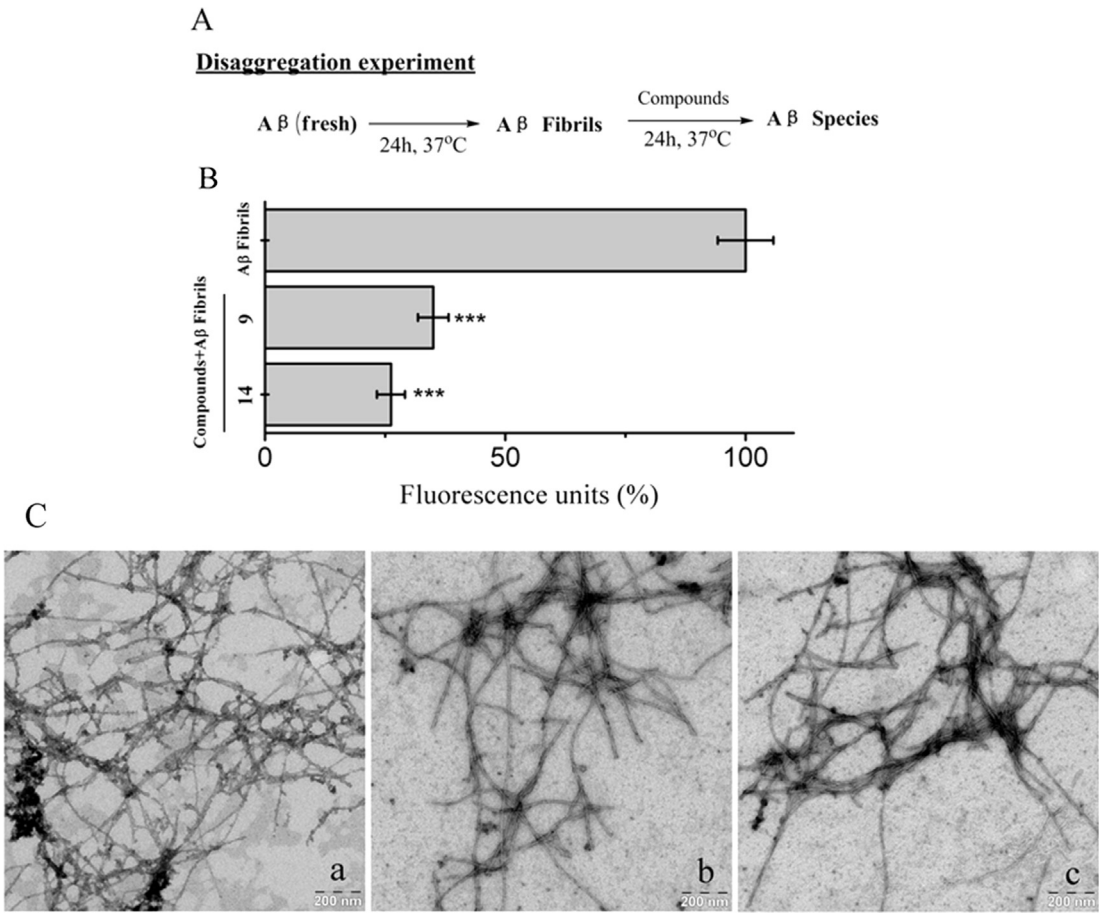

Fig. 6. (A) Schematic of the disaggregation experiments. (B) Results of the ThT binding assay. The statistical significance was analysed by ANOVA. ***$p < 0.001$ versus the control. (C) TEM images ([$A\beta_{1-42}$] = 25 μM, [**9**] = 20 μM, [**14**] = 20 μM, 37 °C, 24 h; (a) $A\beta_{1-42}$ alone, (b) $A\beta_{1-42}$ + **9**, (c) $A\beta_{1-42}$ + **14**).

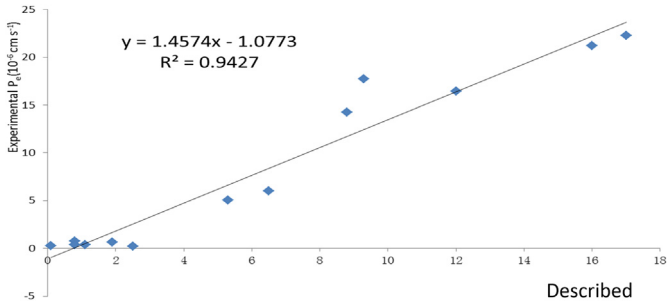

Fig. 7. Linear correlation between the experimental and the reported permeabilities of commercial drugs using the PAMPA-BBB assay. P_e(exp.) = 1.4574*Pe* (bibl.) − 1.0773 (R^2 = 0.9427).

limit established by Di et al. for blood–brain barrier permeation, we classified compounds as follows:

(a) 'CNS+' (high BBB permeation predicted); P_e (10^{-6} cm s^{-1}) > 4.7
(b) 'CNS−' (low BBB permeation predicted); P_e (10^{-6} cm s^{-1}) < 1.8
(c) ' CNS+/−' (BBB permeation uncertain); P_e (10^{-6} cm s^{-1}) from 1.8 to 4.7

Finally, the new synthetic hybrids were then tested through the PAMPA-BBB assay, and the results are presented in Table 3. Among them, compounds **6**, **7**, **8**, **9**, **13**, **14**, **18** could be able to cross the blood–brain barrier (CNS+) and compounds **15**, **17a** were classified as ' CNS+/−' (BBB permeation uncertain).

3. Conclusion

In conclusion, we synthesized and evaluated a series of indanone derivatives as multifunctional anti-AD agents. Our results demonstrate that most of these compounds demonstrated good inhibitory activities against AChE, with IC_{50} values in the nanomolar range. In particular, compounds **9** (IC_{50} = 14.8 nM) and **14** (IC_{50} = 18.6 nM) exhibited markedly higher activities than tacrine and similar activities to donepezil. In addition, **9** and **14** exhibited significant inhibitory activity against Aβ aggregation (inhibition rates of 85.5% and 83.8%, respectively), were able to significantly disaggregate Aβ fibrils generated by self-induced Aβ aggregation, and presented significant antioxidant activity. Furthermore, **9** and **14** can cross the blood–brain barrier (BBB) in vitro. These properties highlight the potential of these new compounds for their development as multi-functional drugs for the treatment of Alzheimer's disease.

Table 3
Permeabilities (P_e × 10^{-6} cm s^{-1}) of the selected compounds measured using the PAMPA-BBB assay and their predicted penetration into the CNS.

Compound[a]	P_e (× 10^{-6} cm s^{-1})[b]	Prediction
6	9.06 ± 0.26	CNS+
7	9.07 ± 0.88	CNS+
8	9.02 ± 0.52	CNS+
9	8.86 ± 0.50	CNS+
13	9.59 ± 0.54	CNS+
14	7.75 ± 0.29	CNS+
15	3.38 ± 0.31	CNS+/−
17a	3.51 ± 0.26	CNS+/−
18	10.52 ± 0.44	CNS+

[a] The compounds were dissolved in DMSO to a concentration of 5 mg mL^{-1} and diluted with PBS/EtOH (70:30).
[b] The values are expressed as the means ± SD of three independent experiments.

4. Experimental section

4.1. Chemistry

The MS spectra were generated using an Agilent LC–MS 6120 instrument with an ESI mass selective detector in the positive ion mode. The melting points were determined using an SRS-Opti Melt automated melting point instrument. The NMR spectra were acquired with a Bruker Avance III spectrometer using TMS as the internal standard. The purities of the synthesized compounds were determined by high-performance liquid chromatography (HPLC) with a TC-C18 column (4.6 × 250 mm, 5 μm), an acetonitrile/water or acetonitrile/water (0.1% TFA) mobile phase, and a flow rate of 1 mL/min.

4.1.1. 3-(4-hydroxy-3-methoxyphenyl)propanoic acid (**2**) [11]

Pd/C (3.75 g) was added to a stirred suspension of ferulic acid (25 g, 128.74 mmol) in methanol (200 ml), and the mixture was hydrogenated at a hydrogen pressure of 1.2 MPa for 4 h at 50 °C. After cooling to room temperature, the mixture was filtered and vacuumed to obtain a white solid (25 g, 99%). ^{1}H NMR (400 MHz, $CDCl_3$) δ 6.76 (d, *J* = 7.8 Hz, 1H), 6.62 (m, 2H), 3.79 (s, 3H), 2.81 (t, *J* = 7.7 Hz, 2H), 2.58 (t, *J* = 7.7 Hz, 2H). ESI-MS *m/z*: 195.1 [M−H].

4.1.2. 6-Hydroxy-5-methoxy-2,3-dihydro-1H-inden-1-one (**3**) [22]

Compound **2** (25 g, 127.4 mmol) was dissolved in a solution of methanesulfonic acid (250 g), and the mixture was stirred at 120 °C for 1 h. After the reaction was completed (monitored by TLC), the mixture was poured into ice water and filtered. The crude product was recrystallized in ethanol to afford a yellow solid (16 g, 65%). ^{1}H NMR (400 MHz, $CDCl_3$) δ 7.25 (s, 1H), 6.88 (s, 1H), 5.73 (s, 1H), 3.99 (s, 3H), 3.04 (m, 2H), 2.66 (m, 2H). ESI-MS *m/z*: 179.1 $[M+H]^+$.

4.1.3. General procedures for the preparation of **4a**–**4d** [11]

α,ω-Dibromoethane was added to a stirred mixture of **3** (2 g, 11.22 mmol) and K_2CO_3 (4.65 g, 33.66 mmol) in acetonitrile. After stirring for 4 h, the mixture was filtered, and the solvent was removed in vacuum to obtain the crude product, which was purified by chromatography on silica gel using petroleum/ethyl acetate (100:1–5:1) as the eluent to afford the target compound.

4.1.4. 6-(2-bromoethoxy)-5-methoxy-2,3-dihydro-1H-inden-1-one (**4a**)

Yield: 50%. ^{1}H NMR (400 MHz, $CDCl_3$) δ 7.20 (s, 1H), 6.92 (s, 1H), 4.35 (t, *J* = 6.5 Hz, 2H), 3.96 (s, 3H), 3.68 (t, *J* = 6.5 Hz, 2H), 3.06 (m, 2H), 2.68 (m, 2H). ESI-MS *m/z*: 285.1 $[M+H]^+$

4.1.5. 6-(3-bromopropoxy)-5-methoxy-2,3-dihydro-1H-inden-1-one (**4b**)

Yield: 60%. ^{1}H NMR (400 MHz, $CDCl_3$) δ 7.21 (s, 1H), 6.89 (s, 1H), 4.17 (t, *J* = 5.9 Hz, 2H), 3.94 (s, 3H), 3.62 (t, *J* = 6.4 Hz, 2H), 3.05 (m, 2H), 2.68 (m, 2H), 2.38 (m, 2H). ESI-MS *m/z*: 299.2 $[M+H]^+$

4.1.6. 6-(4-bromobutoxy)-5-methoxy-2,3-dihydro-1H-inden-1-one (**4c**)

Yield: 67%. ^{1}H NMR (400 MHz, $CDCl_3$) δ 7.20 (s, 1H), 6.89 (s, 1H), 4.09 (t, *J* = 6.6 Hz, 2H), 3.95 (s, 3H), 3.05 (m, 2H), 2.67 (m, 2H), 2.08 (t, *J* = 13.8, 6.7 Hz, 2H), 1.64 (dt, *J* = 11.0, 5.6 Hz, 4H). ESI-MS *m/z*: 313.0 $[M+H]^+$

4.1.7. 6-(5-bromopentyloxy)-5-methoxy-2,3-dihydro-1H-inden-1-one (**4d**)

Yield: 75%. ^{1}H NMR (400 MHz, $CDCl_3$) δ 7.15 (s, 1H), 6.89 (s, 1H), 4.04 (t, *J* = 6.3 Hz, 2H), 3.95 (s, 3H), 3.05 (m, 2H), 2.99 (m, 2H), 2.67

(m, 2H), 2.03 (m, 2H), 1.90 (m, 2H), 1.57 (dt, J = 15.1, 7.6 Hz, 2H). ESI-MS m/z: 327.1 $[M+H]^+$

*4.1.8. General procedures for the preparation of **5a**, **5b**, **5d** [11]*

Piperidine (2.4 mol) was added and the mixture was refluxed for 2 h to a solution of **4** (0.8 mmol) in 20 ml of acetonitrile. After the solvent was removed in vacuum, the crude product was purified on silica gel using petroleum/ethyl acetate as the eluent to obtain compounds **5a**, **5b**, **5d**.

*4.1.9. 5-Methoxy-6-(2-(piperidin-1-yl)ethoxy)-2,3-dihydro-1H-inden-1-one (**5a**)*

Yield: 55%. M.p. 115–117 °C; ^{1}H NMR (400 MHz, $CDCl_3$) δ 7.20 (s, 1H), 6.88 (s, 1H), 4.16 (t, J = 6.2 Hz, 2H), 3.94 (d, J = 5.6 Hz, 3H), 3.05 (m, 2H), 2.83 (dd, J = 10.8, 4.6 Hz, 2H), 2.67 (m, 2H), 2.51 (s, 5H), 1.61 (dt, J = 10.9, 5.6 Hz, 5H). ESI-MS m/z: 290.2 $[M+H]^+$

*4.1.10. 5-Methoxy-6-(3-(piperidin-1-yl)propoxy)-2,3-dihydro-1H-inden-1-one (**5b**)*

Yield: 65%. M.p. 128–129 °C; ^{1}H NMR (400 MHz, $CDCl_3$) δ 7.15 (s, 1H), 6.88 (s, 1H), 4.04 (t, J = 6.2 Hz, 2H), 3.94 (s, 3H), 3.04 (m, 2H), 2.84 (s, 10H), 2.67 (m, 4H), 1.91 (m, 2H). ESI-MS m/z: 304.1 $[M+H]^+$

*4.1.11. 5-Methoxy-6-(5-(piperidin-1-yl)pentyloxy)-2,3-dihydro-1H-inden-1-one (**5d**)*

Yield: 80%. M.p. 115–117 °C; ^{1}H NMR (400 MHz, $CDCl_3$) δ 7.16 (s, 1H), 6.89 (s, 1H), 4.03 (t, J = 6.5 Hz, 2H), 3.95 (s, 3H), 3.05 (m, 2H), 2.67 (m, 6H), 2.60 (d, J = 7.9 Hz, 2H), 1.88 (m, 2H), 1.78 (m, 6H), 1.50 (m, 4H). ESI-MS m/z: 332.2 $[M+H]^+$

4.1.12. General procedures for the preparation of 6–15

Sodium hydroxide (0.35 g, 8.75 mmol) and the appropriate benzaldehyde (3.5 mmol) was added to a solution of **5** (1.75 mmol) in 30 ml of methanol. After the mixture was stirred at room temperature for 2–5 h, the solid was filtered, chromatographed on silica gel, and eluted with petroleum/ethyl acetate (10:1–1:1) as the eluent to afford the proposed compound.

*4.1.13. (E)-2-(4-(dimethylamino)benzylidene)-5-methoxy-6-(2-(piperidin-1-yl)ethoxy)-2,3-dihydro-1H-inden-1-one (**6**)*

Yellow solid; Yield: 87%; M.p. 164.1–165.0 °C; ^{1}H NMR (400 MHz, CDCl3) δ 7.54 (d, J = 9.0 Hz, 3H), 7.33 (s, 1H), 6.95 (s, 1H), 6.71 (d, J = 8.9 Hz, 2H), 4.19 (t, J = 6.2 Hz, 2H), 3.95 (s, 3H), 3.87 (s, 2H), 3.02 (s, 6H), 2.83 (t, J = 6.2 Hz, 2H), 2.51 (s, 4H), 1.61 (dt, J = 11.0, 5.6 Hz, 4H), 1.47–1.40 (m, 2H); ^{13}C NMR (101 MHz, $CDCl_3$) δ 193.21, 155.00, 150.92, 148.65, 144.42, 133.63, 132.44, 131.63, 130.89, 123.31, 111.89, 108.35, 66.35, 58.65, 56.15, 54.86, 40.01, 32.32, 25.85, 24.24. HRMS (ESI) m/z calcd for $C_{26}H_{32}N_2O_3$, 421.2486; found, 421.2504. Purity: 98.8% (by HPLC).

*4.1.14. (E)-2-(4-(dimethylamino)benzylidene)-5-methoxy-6-(3-(piperidin-1-yl)propoxy)-2,3-dihydro-1H-inden-1-one (**7**)*

Yellow solid; Yield: 79%; M.p. 174.6–174.9 °C; ^{1}H NMR (400 MHz, CDCl3) δ 7.66 (m, 3H), 7.35 (s, 1H), 6.97 (s, 1H), 6.74 (d, J = 8.8 Hz, 2H), 4.13 (t, J = 6.7 Hz, 2H), 3.96 (s, 3H), 3.91 (s, 2H), 3.05 (s, 6H), 2.57 (m, 3H), 2.40 (s, 3H), 2.06 (dd, J = 14.0, 6.9 Hz, 2H), 1.64 (m, 4H), 1.44 (d, J = 5.4 Hz, 2H); ^{13}C NMR (101 MHz, $CDCl_3$) δ 193.21, 155.20, 150.96, 148.89, 144.23, 133.22, 132.42, 131.67, 130.80, 123.50, 111.96, 107.44, 67.82, 56.19, 55.79, 54.60, 40.07, 32.35, 26.59, 25.99, 24.47. HRMS (ESI) m/z calcd for $C_{27}H_{34}N_2O_3$, 435.2642; found, 435.2663. Purity: 99.5% (by HPLC).

*4.1.15. (E)-2-(4-(dimethylamino)benzylidene)-5-methoxy-6-(5-(piperidin-1-yl)pentyloxy)-2,3-dihydro-1H-inden-1-one (**8**)*

Yellow solid; Yield: 90%; M.p. 154.0–154.9 °C; ^{1}H NMR (400 MHz, CDCl3) δ 7.61 (m, 3H), 7.33 (s, 1H), 6.96 (s, 1H), 6.74 (d, J = 8.9 Hz, 2H), 4.08 (t, J = 6.8 Hz, 2H), 3.96 (s, 3H), 3.90 (s, 2H), 3.04 (s, 6H), 2.37 (s, 4H), 2.34 (m, 2H), 1.94 (m, 2H), 1.58 (dt, J = 10.9, 5.5 Hz, 6H), 1.45 (dd, J = 12.8, 6.3 Hz, 4H; ^{13}C NMR (101 MHz, $CDCl_3$) δ 193.28, 155.13, 150.90, 148.85, 144.20, 133.18, 132.39, 131.58, 130.71, 123.39, 111.90,107.39, 68.98, 59.37, 56.17, 54.62, 40.01,36.50, 28.95, 26.65, 25.96, 24.48, 24.15. HRMS (ESI) m/z calcd for $C_{29}H_{38}N_2O_3$, 463.2955; found, 463.2978. Purity: 97.7% (by HPLC).

*4.1.16. (E)-2-(4-(diethylamino)benzylidene)-5-methoxy-6-(2-(piperidin-1-yl)ethoxy)-2,3-dihydro-1H-inden-1-one (**9**)*

Yellow solid; Yield: 88%; M.p. 109.1–109.5 °C; ^{1}H NMR (400 MHz, CDCl3) δ 7.61 (m, 3H), 7.38 (s, 1H), 6.98 (d, J = 3.0 Hz, 1H), 6.76 (m, 2H), 4.23 (t, J = 6.3 Hz, 2H), 3.97 (d, J = 7.6 Hz, 3H), 3.89 (d, J = 22.4 Hz, 2H), 3.44 (q, J = 7.1 Hz, 4H), 2.88 (dt, J = 15.8, 6.3 Hz, 2H), 2.59 (m, 4H), 1.62 (dd, J = 10.8, 5.5 Hz, 4H), 1.47 (dd, J = 11.4, 5.9 Hz, 2H), 1.23 (t, J = 7.1 Hz, **13**); ^{13}C NMR (101 MHz, $CDCl_3$) δ 193.27, 154.40, 150.64, 148.89, 144.33, 141.30, 132.79, 131.60, 122.43, 111.41, 107.50, 66.69, 57.58, 56.17, 54.90, 44.44, 32.39, 25.89, 24.22, 12.61. HRMS (ESI) m/z calcd for $C_{28}H_{36}N_2O_3$, 449.2799; found, 449.2817. Purity: 98.5% (by HPLC).

*4.1.17. (E)-2-(4-(diethylamino)benzylidene)-5-methoxy-6-(3-(piperidin-1-yl)propoxy)-2,3-dihydro-1H-inden-1-one (**10**)*

Yellow solid; Yield: 74%; M.p. 155.2–155.4 °C; ^{1}H NMR (400 MHz, CDCl3) δ 7.57 (d, J = 9.1 Hz, 3H), 7.37 (s, 1H), 6.98 (s, 1H), 6.72 (d, J = 8.9 Hz, 2H), 4.15 (t, J = 6.7 Hz, 2H), 3.98 (s, 3H), 3.92 (s, 2H), 3.44 (q, J = 7.1 Hz, 4H), 2.55 (m, 2H), 2.41 (s, 4H), 2.06 (dt, J = 13.9, 6.8 Hz, 2H), 1.62 (m, 6H), 1.22 (t, J = 7.1 Hz, 6H); ^{13}C NMR (101 MHz, $CDCl_3$) δ 193.25, 155.09, 148.83, 148.54, 144.16, 133.29, 132.74, 131.69, 122.57, 111.38, 107.45, 67.77, 56.15, 55.77, 54.58, 44.40, 32.35, 26.59, 25.98, 24.46, 12.61. HRMS (ESI) m/z calcd for $C_{29}H_{38}N_2O_3$, 463.2955; found, 463.2968 Purity: 99.1% (by HPLC).

*4.1.18. (E)-2-(4-(diethylamino)benzylidene)-5-methoxy-6-(5-(piperidin-1-yl)pentyloxy)-2,3-dihydro-1H-inden-1-one (**11**)*

Yellow solid; Yield: 81%; M.p. 141.6–142.3 °C; ^{1}H NMR (400 MHz, CDCl3) δ 7.55 (d, J = 9.1 Hz, 3H), 7.33 (s, 1H), 6.96 (s, 1H), 6.70 (d, J = 8.9 Hz, 2H), 4.08 (t, J = 6.8 Hz, 2H), 3.97 (s, 3H), 3.90 (s, 2H), 3.42 (q, J = 7.0 Hz, 4H), 2.45 (m, 6H), 1.94 (m, 2H), 1.60 (m, 6H), 1.52 (m, 4H), 1.21 (t, J = 7.1 Hz, 6H); ^{13}C NMR (101 MHz, $CDCl_3$) δ 193.33, 155.08, 148.86, 148.57, 144.11, 133.33, 132.77, 131.73, 122.62, 111.40, 107.41, 69.01, 59.38, 56.19, 54.62, 44.43, 32.38, 28.95, 26.64, 25.96, 24.48, 24.16, 12.61. HRMS (ESI) m/z calcd for $C_{31}H_{42}N_2O_3$, 491.3268; found, 491.3288 Purity: 96.1% (by HPLC).

*4.1.19. (E)-5-methoxy-2-(4-(methylamino)benzylidene)-6-(2-(piperidin-1-yl)ethoxy)-2,3-dihydro-1H-inden-1-one (**12**)*

Yellow solid; Yield: 85%; M.p. 175.5–176.2 °C; ^{1}H NMR (400 MHz, CDCl3) δ 7.52 (d, J = 8.3 Hz, 3H), 7.35 (s, 1H), 6.96 (s, 1H), 6.63 (d, J = 8.7 Hz, 2H), 4.20 (t, J = 6.2 Hz, 2H), 4.12 (d, J = 4.6 Hz, 1H), 3.96 (s, 3H), 3.90 (s, 2H), 2.90 (d, J = 4.9 Hz, 3H), 2.84 (t, J = 6.2 Hz, 2H), 2.54–2.50 (m, 3H), 1.93 (s, 3H), 1.62 (dt, J = 11.0, 5.7 Hz, 4H); ^{13}C NMR (101 MHz, $CDCl_3$) δ 193.29, 155.17, 150.39, 148.75, 144.44, 133.32, 132.60, 131.61, 130.77, 124.47, 112.23, 107.47, 66.74, 57.58, 56.17, 54.92, 32.34, 30.22, 25.90, 24.21. HRMS (ESI) m/z calcd for $C_{25}H_{30}N_2O_3$, 407.2329; found, 407.2334 Purity: 99.8% (by HPLC).

*4.1.20. (E)-2-(4-(ethyl(methyl)amino)benzylidene)-5-methoxy-6-(2-(piperidin-1-yl)ethoxy)-2,3-dihydro-1H-inden-1-one (**13**)*

Yellow solid; Yield: 66%; M.p. 132.0–132.9 °C; ^{1}H NMR (400 MHz, $CDCl_3$) δ 7.47 (d, *J* = 9.1 Hz, 3H), 7.28 (s, 1H), 6.88 (s, 1H), 6.64 (d, *J* = 8.9 Hz, 2H), 4.13 (t, *J* = 6.3 Hz, 2H), 3.91–3.86 (m, 3H), 3.81 (s, 2H), 3.43–3.35 (m, 2H), 2.94–2.88 (m, 3H), 2.78 (t, *J* = 6.3 Hz, 2H), 2.45 (s, 4H), 1.53 (dd, *J* = 11.0, 5.5 Hz, 4H), 1.38 (d, *J* = 5.2 Hz, 2H), 1.09 (t, *J* = 7.1 Hz, 3H). ^{13}C NMR (101 MHz, $CDCl_3$) δ 193.26, 155.11, 149.72, 148.72, 144.38, 133.32, 132.62, 131.72, 130.45, 123.07, 111.77, 107.48, 106.55, 66.82, 57.57, 56.18, 54.93, 46.56, 37.38, 32.37, 25.92, 24.21, 11.49. HRMS (ESI) *m*/*z* calcd for $C_{27}H_{34}N_2O_3$, 435.2642; found, 435.2663 Purity: 96.5% (by HPLC).

*4.1.21. (E)-5-methoxy-2-(4-(methyl(propyl)amino)benzylidene)-6-(2-(piperidin-1-yl)ethoxy)-2,3-dihydro-1H-inden-1-one (**14**)*

Yellow solid; Yield: 70%; M.p. 123.0–123.8 °C; ^{1}H NMR (400 MHz, $CDCl_3$) δ 7.54 (d, *J* = 6.4 Hz, 3H), 7.35 (d, *J* = 2.0 Hz, 1H), 6.96 (s, 1H), 6.73–6.65 (m, 2H), 4.21 (dd, *J* = 6.0, 3.9 Hz, 2H), 3.95 (d, *J* = 2.2 Hz, 3H), 3.88 (s, 2H), 3.34 (t, *J* = 6.2 Hz, 2H), 3.01 (d, *J* = 2.2 Hz, 3H), 2.85 (dd, *J* = 5.9, 3.8 Hz, 2H), 2.53 (s, 4H), 1.62 (d, *J* = 4.8 Hz, 6H), 1.45 (s, 2H), 0.94 (td, *J* = 7.2, 2.2 Hz, 3H). ^{13}C NMR (101 MHz, $CDCl_3$) δ 193.26, 155.06, 150.00, 148.69, 144.37, 133.37, 132.59, 131.74, 130.36, 122.94, 111.64, 107.48, 106.49, 66.66, 57.57, 56.17, 54.90, 54.10, 38.37, 32.38, 25.87, 24.20, 20.16, 11.43. HRMS (ESI) *m*/*z* calcd for $C_{28}H_{36}N_2O_3$, 449.2799; found, 449.2817 Purity: 96.9% (by HPLC).

*4.1.22. (E)-2-(4-(dipropylamino)benzylidene)-5-methoxy-6-(2-(piperidin-1-yl)ethoxy)-2,3-dihydro-1H-inden-1-one (**15**)*

Yellow solid; Yield: 76%; M.p. 128.0–128.9 °C; ^{1}H NMR (400 MHz, $CDCl_3$) δ 7.54 (d, *J* = 7.5 Hz, 3H), 7.36 (s, 1H), 6.96 (s, 1H), 6.67 (d, *J* = 8.3 Hz, 2H), 4.21 (t, *J* = 6.3 Hz, 2H), 3.95 (d, *J* = 8.0 Hz, 3H), 3.90 (s, 2H), 3.34–3.27 (m, 4H), 2.85 (t, *J* = 6.2 Hz, 2H), 2.52 (s, 4H), 1.68–1.59 (m, 8H), 1.45 (d, *J* = 4.8 Hz, 2H), 0.96 (t, *J* = 7.3 Hz, 6H). ^{13}C NMR (101 MHz, $CDCl_3$) δ 193.27, 155.00, 149.02, 148.67, 144.32, 133.41, 132.71, 131.77, 130.07, 122.49, 111.48, 107.46, 106.44, 66.67, 57.57, 56.17, 54.90, 52.75, 32.40, 25.90, 24.22, 20.47, 11.38. HRMS (ESI) *m*/*z* calcd for $C_{30}H_{40}N_2O_3$, 477.3112; found, 477.3123 Purity: 96.6% (by HPLC).

*4.1.23. General procedures for the preparation of **16a**–**16c***

Cyclohexylamine (2.4 mol) was added to a solution of **4** (0.8 mmol) in 20 ml of acetonitrile, and the mixture was refluxed for 2 h. After the solvent was removed in vacuum, the crude product was purified on silica gel using petroleum/ethyl acetate as the eluent to give compounds **16a**–**16c**.

*4.1.24. 6-(2-(cyclohexylamino)ethoxy)-5-methoxy-2,3-dihydro-1H-inden-1-one (**16a**)*

Yield: 50%. ^{1}H NMR (400 MHz, CDCl3) δ 7.19 (m, 1H), 6.89 (m, 1H), 4.01 (t, *J* = 5.3 Hz, 2H), 3.82 (s, 3H), 3.05 (m, 4H), 2.60 (m, 2H), 2.39 (dd, *J* = 21.1, 7.0 Hz, 1H), 2.14 (s, 1H), 1.80 (d, *J* = 10.4 Hz, 2H), 1.63 (dd, *J* = 11.1, 5.2 Hz, 2H), 1.23 (m, 7H). ESI-MS *m*/*z*: 304.2 $[M+H]^+$

*4.1.25. 6-(3-(cyclohexylamino)propoxy)-5-methoxy-2,3-dihydro-1H-inden-1-one (**16b**)*

Yield: 62%. ^{1}H NMR (400 MHz, CDCl3) δ 7.17 (s, 1H), 6.94 (s, 1H), 4.21 (t, *J* = 5.5 Hz, 2H), 3.99 (s, 3H), 3.33 (t, *J* = 5.7 Hz, 2H), 3.10 (m, 2H), 2.72 (m, 2H), 2.44 (dt, *J* = 12.0, 6.2 Hz, 2H), 2.25 (d, *J* = 11.3 Hz, 2H), 1.71 (d, *J* = 14.8 Hz, 2H), 1.65 (d, *J* = 11.3 Hz, 2H), 1.29 (dd, *J* = 21.5, 9.0 Hz, 6H). ESI-MS *m*/*z*: 318.2 $[M+H]^+$

*4.1.26. 6-(4-(cyclohexylamino)butoxy)-5-methoxy-2,3-dihydro-1H-inden-1-one (**16c**)*

Yield: 70%. ^{1}H NMR (400 MHz, CDCl3) δ 7.20 (s, 1H), 6.88 (s, 1H), 4.09 (dt, *J* = 9.8, 4.9 Hz, 2H), 3.94 (s, 3H), 3.11 (m, 2H), 2.67 (dd, *J* = 9.7, 4.0 Hz, 2H), 2.55 (m, 7H), 2.03 (dt, *J* = 13.1, 6.6 Hz, 2H), 1.63 (s, 5H), 1.60 (m, 4H). ESI-MS *m*/*z*: 332.1 $[M+H]^+$

*4.1.27. General procedures for the preparation of **17a**–**17c***

Sodium hydroxide (0.35 g, 8.75 mmol) and 4-(dimethylamino) benzaldehyde (3.5 mmol) were added to a solution of **16** (1.75 mmol) in methanol. After the mixture was stirred at room temperature for 2–5 h, the solid was filtered, chromatographed on silica gel, and eluted with petroleum/ethyl acetate (10:1–1:1) as the eluent to afford the proposed compound.

*4.1.28. (E)-6-(2-(cyclohexylamino)ethoxy)-2-(4-(dimethylamino) benzylidene)-5-methoxy-2,3-dihydro-1H-inden-1-one (**17a**)*

Yellow solid; Yield: 75%; M.p. 143.5–144.3 °C; ^{1}H NMR (400 MHz, CDCl3) δ 7.57 (d, *J* = 9.1 Hz, 3H), 7.36 (s, 1H), 6.97 (s, 1H), 6.74 (d, *J* = 8.7 Hz, 2H), 4.20 (m, 2H), 3.96 (d, *J* = 4.2 Hz, 3H), 3.89 (d, *J* = 21.4 Hz, 2H), 3.12 (m, 2H), 3.05 (s, 6H), 2.49 (d, *J* = 8.2 Hz, 1H), 1.75 (d, *J* = 9.1 Hz, 2H), 1.38 (m, 8H); ^{13}C NMR (101 MHz, $CDCl_3$) δ 193.21, 155.20, 150.92, 148.66, 144.59, 133.31, 132.45, 131.58, 130.87, 123.30, 111.88, 108.44, 65.51, 56.59, 56.08, 46.85, 45.55, 39.99, 33.41, 26.14, 25.00. HRMS (ESI) *m*/*z* calcd for $C_{27}H_{34}N_2O_3$, 435.2642; found, 435.2659 Purity: 98.0% (by HPLC).

*4.1.29. (E)-6-(3-(cyclohexylamino)propoxy)-2-(4-(dimethylamino) benzylidene)-5-methoxy-2,3-dihydro-1H-inden-1-one (**17b**)*

Yellow solid; Yield: 80%; M.p. 108.9–109.7 °C; ^{1}H NMR (400 MHz, CDCl3) δ 7.57 (d, *J* = 8.9 Hz, 3H), 7.34 (s, 1H), 6.97 (s, 1H), 6.74 (d, *J* = 8.7 Hz, 2H), 4.16 (t, *J* = 6.2 Hz, 2H), 3.96 (s, 3H), 3.91 (s, 2H), 3.04 (s, 6H), 2.87 (t, *J* = 6.7 Hz, 2H), 2.57 (m, 1H), 2.11 (m, 2H), 1.91 (d, *J* = 12.1 Hz, 2H), 1.74 (dd, *J* = 12.1, 4.1 Hz, 2H), 1.62 (d, *J* = 11.7 Hz, 1H), 1.34 (m, 6H); ^{13}C NMR (101 MHz, $CDCl_3$) δ 192.38, 155.12, 150.99, 148.70, 144.41, 133.33, 132.45, 130.79, 128.82, 123.31, 111.96, 107.45, 68.12, 56.76, 56.14, 44.15, 40.07, 33.16, 32.37, 30.56, 26.08, 25.02.ESI-MS *m*/*z*: 449.3 $[M+H]^+$

HRMS (ESI) *m*/*z* calcd for $C_{28}H_{36}N_2O_3$, 449.2799; found, 449.2821 Purity: 97.1% (by HPLC).

*4.1.30. (E)-6-(4-(cyclohexylamino)butoxy)-2-(4-(dimethylamino) benzylidene)-5-methoxy-2,3-dihydro-1H-inden-1-one (**17c**)*

Yellow solid; Yield: 82%; M.p. 146.5–147.1 °C; ^{1}H NMR (400 MHz, CDCl3) δ 7.46 (d, *J* = 9.0 Hz, 3H), 7.23 (s, 1H), 6.87 (s, 1H), 6.63 (d, *J* = 8.8 Hz, 2H), 4.00 (t, *J* = 6.6 Hz, 2H), 3.92 (m, 3H), 3.78 (s, 2H), 2.94 (s, 6H), 2.62 (t, *J* = 7.2 Hz, 2H), 2.43 (m, 1H), 1.87 (m, 4H), 1.68 (m, 4H), 1.08 (ddt, *J* = 37.6, 24.6, 12.3 Hz, 6H); ^{13}C NMR (101 MHz, $CDCl_3$) δ 193.30, 155.15, 150.95, 148.80, 144.24, 133.23, 132.42, 131.61, 130.74, 123.45, 111.94, 107.40, 68.88, 56.81, 56.17, 46.53, 40.05, 33.58, 32.34, 26.95, 26.17, 25.08. HRMS (ESI) *m*/*z* calcd for $C_{29}H_{38}N_2O_3$, 463.2955; found, 463.2978 Purity: 99.3% (by HPLC).

*4.1.31. (E)-5-methoxy-2-(4-methoxybenzylidene)-6-(2-(piperidin-1-yl)ethoxy)-2,3-dihydro-1H-inden-1-one (**18**)*

To a solution of **5a** (1.75 mmol) in methanol, sodium hydroxide (0.35 g, 8.75 mmol) and 4-methoxybenzaldehyde (3.5 mmol) was added. After the mixture was stirred at room temperature for 2–5 h, the solid was filtered, and chromatographed on silica gel and eluted with Petroleum/ethyl acetate (10:1–1:1) as an eluent to afford the proposed compound.

Yellow solid; Yield: 86%; M.p. 137.3–138.2 °C; ^{1}H NMR (400 MHz, $CDCl_3$) δ 7.61 (d, *J* = 8.6 Hz, 2H), 7.56 (s, 1H), 7.36 (s, 1H), 6.97 (d, *J* = 6.1 Hz, 3H), 4.21 (t, *J* = 6.2 Hz, 2H), 3.97 (s, 3H), 3.92 (s, 2H), 3.86 (s, 3H), 2.85 (t, *J* = 6.2 Hz, 2H), 2.53 (s, 4H), 1.61 (s, 4H), 1.45

(d, J = 4.4 Hz, 2H). ^{13}C NMR (101 MHz, $CDCl_3$) δ 193.14, 160.58, 155.55, 148.90, 144.65, 133.21, 132.25, 132.13, 131.24, 128.36, 114.39, 107.42, 106.58, 66.88, 57.56, 56.21, 55.35, 54.96, 32.14, 25.93, 24.21. HRMS (ESI) m/z calcd for $C_{25}H_{29}NO_4$, 408.2188; found, 408.2169 Purity: 96.9% (by HPLC).

4.2. Biological assays

4.2.1. In vitro inhibition of ChEs

Acetylcholinesterase (AChE, E.C. 3.1.1.7, from electric eel or human erythrocytes), butyrylcholinesterase (BuChE, E.C. 3.1.1.8, from equine serum), 5,5'-dithiobis-(2-nitrobenzoic acid) (Ellman's reagent, DTNB), acetylthiocholine chloride (ATC), and butylthiocholine chloride (BTC) were purchased from Sigma Aldrich. The prototypes tacrine and donepezil were used as reference compounds. Five different concentrations of each compound were used to obtain between 20% and 80% inhibition of cholinesterase activity.

All in vitro AChE assays were performed in 0.1 M KH_2PO_4/K_2HPO_4 buffer, pH 8.0, using a Shimadzu UV-2450 spectrophotometer. The AChE solutions were prepared to obtain 2.0 units/ml in 2-ml aliquots. The assay medium (1 mL) consisted of phosphate buffer (pH 8.0), 50 μl of 0.01 M DTNB, 10 μl of the enzyme, and 50 μl of the substrate at a concentration of 0.01 M. The test compounds were added to the assay solution and pre-incubated with the enzyme at 37 °C for 15 min prior to the addition of the substrate. The activity was determined by measuring the increase in the absorbance of the mixture at 412 nm at 1-min intervals at 37 °C. The calculations were performed according to the method described by Ellman et al.[15]. Each concentration was assayed in triplicate. Blanks containing all of the components except AChE were included in the analyses. The percent inhibition was calculated by the following expression: $(1 - A_i/A_c) \times 100\%$, where A_i and A_c are the absorbances obtained for AChE in the presence and absence of the inhibitors, respectively, after subtracting the respective background.

The in vitro BuChE assay (using BuChE or ACh as the enzyme substrate) was performed using a method similar to that described above.

4.2.2. Kinetic study of AChE

Kinetic study of AChE was performed using a re-ported method [23]. Test compound was added into the assay solution and pre-incubated with the enzyme at 37 °C for 15 min, followed by the addition of substrate. Kinetic characterization of the hydrolysis of ATC catalysed by AChE was carried out spectro-metrically at 412 nm. A parallel control was made with the assay solution of no inhibitor for each times. The plots were assessed by a weighted least square analysis that assumed the variance of V to be a constant percentage of V for the entire data set. Slopes of these reciprocal plots were then plotted against the concentration of the inhibitors in a weighted analysis and Ki was determined as the ratio of the replot intercept to the replot slope.

4.2.3. Docking study

The simulation system was built based on the structure obtained from the Protein Data Bank (PDB 2CMF for AChE). The heteroatoms and water molecules were removed, and all hydrogen atoms were subsequently added to the protein. Then forcefield was assigned to the enzyme. The ligand binding site was defined as 13 Å from the original ligand. Prior to the docking calculations, the original ligand was removed. The 3D structures of **9**, **10**, **11**, **14** and **17a** were generated and optimized with the Discovery Studio 2.1 package (Accelrys Inc., San Diego, CA).

The CDOCKER program of the Discovery Studio 2.1 software, which allows full flexibility of ligands, was used to perform docking simulations. The docking and subsequent scoring were performed using the default parameters of the CDOCKER program. CDOCKER_INTERACTION_ENERGY is used like a score where a lower value indicates a more favourable binding.

4.2.4. Oxygen radical absorbance capacity (ORAC-FL) assay [24]

The tested compounds and the fluorescein (FL) stock solution were diluted with 75 mM phosphate buffer (pH 7.4) to 10 μM and 0.117 μM, respectively. The solution of (±)-6-hydroxy-2,5,7,8-tetramethylchroman-2-carboxylic acid (Trolox) was diluted with the same buffer to 100, 80, 60, 50, 40, 20, and 10 μM. A solution of 2,2'-azobis-(amidinopropane)dihydrochloride (AAPH) was prepared before the experiment by dissolving 108.4 mg of AAPH in 10 ml of 75 mM phosphate buffer (pH 7.4) to a final concentration of 40 mM. The mixture of the tested compound (20 μl) and FL (120 μl; 70 nM, final concentration) was pre-incubated for 10 min at 37 °C, and 60 μl of the AAPH solution was then added to the mixture. The fluorescence was recorded every minute for a period of 120 min (excitation, 485 nm; emission, 520 nm). A blank using phosphate buffer instead of the tested compound was also carried out. All of the reaction mixtures were prepared in triplicate, and at least three independent runs were performed for each sample. The antioxidant curves (fluorescence versus time) were normalized to the curve of the blank. The area under the fluorescence decay curve (AUC) was calculated using the following equation:

$$\mathrm{AUC} = 1 + \sum_{i=1}^{i=120} (\mathrm{fi}/\mathrm{f0}),$$

where f0 is the initial fluorescence reading at 0 min and fi is the fluorescence reading at time i. The net AUC was calculated by the following equation: $\mathrm{AUC}_{\mathrm{sample}} - \mathrm{AUC}_{\mathrm{blank}}$. The regression equations between the net AUC and the Trolox concentrations were calculated. The ORAC-FL value for each sample was calculated using the standard curve, and the ORAC-FL value of each tested compound is thus expressed as Trolox equivalents.

4.2.5. ThT assay

$A\beta_{1-42}$ (Millipore, counter ion: NaOH) was dissolved in ammonium hydroxide (1% v/v) to obtain a stock solution (2000 μM) that was aliquoted into small samples and stored at −80 °C.

For the experiment to measure the inhibition of self-mediated $A\beta_{1-42}$ aggregation, the Aβ stock solution was diluted with 50 mM phosphate buffer (pH 7.4) to 50 μM before use. A mixture of the peptide (10 μl, 25 μM, final concentration) with or without the tested compound (10 μl, final concentration of 20 μM) was incubated at 37 °C for 48 h. Blanks using 50 mM phosphate buffer (pH 7.4) instead of Aβ with or without the inhibitors were also included in the analyses. The sample was diluted to a final volume of 200 μl with 50 mM glycine–NaOH buffer (pH 8.0) containing thioflavin T (5 μM). The fluorescence intensities were recorded five minutes later (excitation, 450 nm; emission, 485 nm). The percent inhibition of aggregation was calculated using the following expression: $(1 - \mathrm{IF_i}/\mathrm{IF_c}) \times 100\%$, where $\mathrm{IF_i}$ and $\mathrm{IF_c}$ are the fluorescence intensities obtained for Aβ in the presence and absence of the inhibitors after subtracting the background, respectively.

For the experiment to study the disaggregation of self-induced Aβ fibrils, the Aβ stock solution was diluted with 10 mM phosphate buffer (pH 7.4). The peptide (15 μl, 50 μM) was incubated at 37 °C for 24 h. The tested compound (15 μl, 50 μM) was then added, and the mixture incubated at 37 °C for another 24 h. Then, 20 μl of the sample was diluted to a final volume of 200 μl with 50 mM glycine–NaOH buffer (pH 8.0) containing thioflavin T (5 μM). The detection method used was the same as that described above.

4.2.6. TEM assay [25]

The Aβ stock solution was diluted with 10 mM phosphate buffer (pH 7.4), and the sample preparation procedure was the same as that used for the ThT assay. Aliquots (10 μl) of the samples were placed on a carbon-coated copper/rhodium grid for 2 min. Each grid was stained with uranyl acetate (1%, 5 μl) for 2 min. After draining off the excess staining solution, the specimen was transferred for imaging by transmission electron microscopy (JEOL JEM-1400). All of the compounds were solubilized in the buffer that was used for the experiment.

4.2.7. In vitro blood–brain barrier permeation assay

The blood–brain barrier penetration ability of the compounds was evaluated using the parallel artificial membrane permeation assay (PAMPA) described by Di et al. The commercial drugs were purchased from Sigma and Alfa Aesar. Porcine brain lipid (PBL) was obtained from Avanti Polar Lipids. The donor microplate (PVDF membrane, pore size of 0.45 mm) and acceptor microplate were purchased from Millipore. The 96-well UV plate (COSTAR®) was obtained from Corning Incorporated. The acceptor 96-well microplate was filled with 300 μl of PBS/EtOH (7:3), and the filter membrane was impregnated with 4 μl of PBL in dodecane (20 mg/ml). The compounds were dissolved in DMSO at a concentration of 5 mg/ml and diluted 50-fold in PBS/EtOH (7:3) to a final concentration of 100 μg/ml. Then, 200 μl of the solution was added to the donor wells. The acceptor filter plate was carefully placed on the donor plate to form a sandwich, and the plates were incubated undisturbed for 10 h at 25 °C. After incubation, the donor plate was carefully removed, and the concentration of the compounds in the acceptor wells was determined using a UV plate reader (Flexstation® 3). Each sample was analysed at five wavelengths in four wells and in at least three independent runs. P_e was calculated by the following expression: $P_e = -V_d \times V_a/[(V_d + V_a)A \times t] \times \ln(1 - \text{drug}_{\text{acceptor}}/\text{drug}_{\text{equilibrium}})$, where V_d is the volume of the donor well, V_a is the volume of the acceptor well, A is the filter area, t is the permeation time, $\text{drug}_{\text{acceptor}}$ is the absorbance obtained in the acceptor well, and $\text{drug}_{\text{equilibrium}}$ is the theoretical equilibrium absorbance. The results are given as the mean ± standard deviation. In the experiment, 13 quality control standards with known BBB permeabilities were included to validate the analysis set. A plot of the experimental data versus the literature values gave a strong linear correlation: P_e (exp.) = 1.4574Pe (lit.) − 1.0773 (R^2 = 0.9427). From this equation and the limit established by Di et al. (Pe (lit.) = 4.0×10^{-6} cm/s) for blood–brain barrier permeation, we concluded that compounds with a permeability greater than 4.7×10^{-6} cm/s can cross the blood–brain barrier.

Acknowledgement

We thank the National Natural Science Foundation of China (No. 21302235, 20972198), the Opening Project of Guangdong Provincial Key Laboratory of New Drug Design and Evaluation (2011A060901014), Ph.D. Programs Foundation of Ministry of Education of China (20120171120045), and Distinguished Young Talents in Higher Education of Guangdong (2012LYM_003) for financial support of this study.

Appendix A. Supplementary data

Supplementary data related to this article can be found at http://dx.doi.org/10.1016/j.ejmech.2014.09.081.

References

[1] (a) J.B. Standridge, Clin. Ther. 26 (2004) 615–630;
(b) E.D. Roberson, L. Mucke, Science 314 (2006) 781–784.
[2] V.H. Finder, J. Alzheimers Dis. 22 (2010) 5–19.
[3] (a) A. Enz, R. Amstutz, H. Boddeke, G. Gmelin, J. Malanowski, Prog. Brain Res. 98 (1993) 431–438;
(b) P.T. Francis, A.M. Palmer, M. Snape, G.K. Wilcock, J. Neurol. Neurosur. Ps. 66 (1999) 137–147.
[4] G. Pepeu, M.G. Giovannini, Curr. Alzheimer Res. 6 (2009) 86–96.
[5] (a) J. Hardy, J. Neurochem. 110 (2009) 1129–1134;
(b) J.A. Hardy, G.A. Higgins, Science 256 (1992) 184–185;
(c) G. Perry, A. Nunomura, A.K. Raina, G. Aliev, S.L. Siedlak, P.L.R. Harris, G. Casadesus, R.B. Petersen, W. Bligh-Glover, E. Balraj, G.J. Petot, M.A. Smith, Neurochem. Res. 28 (2003) 1549–1552.
[6] S. Salomone, F. Caraci, G.M. Leggio, J. Fedotova, F. Drago, Br. J. Clin. Pharm. 73 (2012) 504–517.
[7] (a) G. Casadesus, P.I. Moreira, A. Nunomura, S.L. Siedlak, W. Bligh-Glover, E. Balraj, G. Petot, M.A. Smith, G. Perry, Neurochem. Res. 32 (2007) 717–722;
(b) F. Gu, M. Zhu, J. Shi, Y. Hu, Z. Zhao, Neurosci. Lett. 440 (2008) 44–48.
[8] (a) K. Hensley, N. Hall, R. Subramaniam, P. Cole, M. Harris, M. Aksenov, M. Aksenova, S.P. Gabbita, J.F. Wu, J.M. Carney, M. Lovell, W.R. Markesbery, D.A. Butterfield, J. Neurochem. 65 (1995) 2146–2156;
(b) W.R. Markesbery, Free Radic. Biol. Med. 23 (1997) 134–147;
(c) M. Padurariu, A. Ciobica, R. Lefter, I.L. Serban, C. Stefanescu, R. Chirita, Psychiatr. Danub. 25 (2013) 401–409.
[9] D. Pratico, Trends Pharmacol. Sci. 29 (2008) 609–615.
[10] (a) M. Rosini, V. Andrisano, M. Bartolini, M.L. Bolognesi, P. Hrelia, A. Minarini, A. Tarozzi, C. Melchiorre, J. Med. Chem. 48 (2005) 360–363;
(b) J. Marco-Contelles, R. León, C. de los Ríos, A. Guglietta, J. Terencio, M.G. López, A.G. García, M. Villarroya, J. Med. Chem. 49 (2006) 7607–7610;
(c) M.L. Bolognesi, A. Cavalli, L. Valgimigli, M. Bartolini, M. Rosini, V. Andrisano, M. Recanatini, C. Melchiorre, J. Med. Chem. 50 (2007) 6446–6449;
(d) M. Rosini, E. Simoni, M. Bartolini, A. Cavalli, L. Ceccarini, N. Pascu, D.W. McClymont, A. Tarozzi, M.L. Bolognesi, A. Minarini, V. Tumiatti, V. Andrisano, I.R. Mellor, C. Melchiorre, J. Med. Chem. 51 (2008) 4381–4384;
(e) J.A. Lenhart, X. Ling, R. Gandhi, T.L. Guo, P.M. Gerk, D.H. Brunzell, S. Zhang, J. Med. Chem. 53 (2010) 6198–6209;
(f) R. Leon, J. Marco-Contelles, Curr. Med. Chem. 18 (2011) 552–576;
(g) M.I. Fernández-Bachiller, C. Pérez, L. Monjas, J. Rademann, M.I. Rodríguez-Franco, J. Med. Chem. 55 (2012) 1303–1317.
[11] F.-C. Meng, F. Mao, W.-J. Shan, F. Qin, L. Huang, X.-S. Li, Bioorg. Med. Chem. Lett. 22 (2012) 4462–4466.
[12] L. Huang, C. Lu, Y. Sun, F. Mao, Z. Luo, T. Su, H. Jiang, W. Shan, X. Li, J. Med. Chem. 55 (2012) 8483–8492.
[13] L. Tian, Z. Hu, P. Shi, H. Zhou, J. Wu, Y. Tian, Y. Zhou, X. Tao, M. Jiang, J. Lumin. 127 (2007) 423–430.
[14] (a) R. Bansal, G. Narang, C. Zimmer, R. Hartmann, Med. Chem. Res. 20 (2011) 661–669;
(b) P.V. Vasuki G, K. Ramamurthi, S.M. Coumar, D.P. Jindal, Acta Cryst. E58 (2002) o1222–o1226;
(c) Z.-B. Cheng, Y.-L. Deng, C.-Q. Fan, Q.-H. Han, S.-L. Lin, G.-H. Tang, H.-B. Luo, S. Yin, J. Nat. Prod. 77 (2014) 180–184.
[15] G.L. Ellman, K.D. Courtney, V. Andres jr, R.M. Featherstone, Biochem. Pharmacol. 7 (1961) 88–95.
[16] (a) B. Ou, D. Huang, M. Hampsch-Woodill, J.A. Flanagan, E.K. Deemer, J. Agric. Food Chem. 50 (2002) 3122–3128;
(b) G. Cao, H.M. Alessio, R.G. Cutler, Free Radic. Biol. Med. 14 (1993) 303–311.
[17] A. Dávalos, C. Gómez-Cordovés, B. Bartolomé, J. Agric. Food Chem. 52 (2003) 48–54.
[18] (a) N. Suzuki, T.T. Cheung, X.D. Cai, A. Odaka, L. Otvos Jr., C. Eckman, T.E. Golde, S.G. Younkin, Science 264 (1994) 1336–1340;
(b) K.N. Dahlgren, A.M. Manelli, W.B. Stine, L.K. Baker, G.A. Krafft, M.J. LaDu, J. Biol. Chem. 277 (2002) 32046–32053.
[19] A. Lorenzo, B.A. Yankner, Proc. Natl. Acad. Sci. U. S. A. 91 (1994) 12243–12247.
[20] E.H. Kerns, L. Di, Curr. Topic Med. Chem. 2 (2002) 87–98.
[21] (a) L. Di, E.H. Kerns, K. Fan, O.J. McConnell, G.T. Carter, Eur. J. Med. Chem. 38 (2003) 223–232;
(b) P. Camps, X. Formosa, C. Galdeano, D. Muñoz-Torrero, L. Ramirez, E. Gomez, N. s. Isambert, R. Lavilla, A. Badia, M. V. r. Clos, M. Bartolini, F. Mancini, V. Andrisano, M.P. Arce, M.I. Rodriguez-Franco, O. s. Huertas, T. Dafni, F.J. Luque, J. Med. Chem. 52 (2009) 5365–5379.
[22] R.V. Heinzelmann, H.G. Kolloff, J.H. Hunter, J. Am. Chem. Soc. 70 (1948) 1386–1390.
[23] M.L. Bolognesi, V. Andrisano, M. Bartolini, R. Banzi, C. Melchiorre, J. Med. Chem. 48 (2004) 24–27.
[24] (a) M.I. Rodríguez-Franco, M.I. Fernández-Bachiller, C. Pérez, B. Hernández-Ledesma, B. Bartolomé, J. Med. Chem. 49 (2006) 459–462;
(b) M. Decker, B. Kraus, J. Heilmann, Bioorg. Med. Chem. 16 (2008) 4252–4261.
[25] J.-S. Choi, J.J. Braymer, R.P.R. Nanga, A. Ramamoorthy, M.H. Lim, Proc. Natl. Acad. Sci. U. S. A. 107 (2010) 21990–21995.